VIRTUAL AIRCRAFT MODEL FOR AEROELASTIC SIMULATION AND LOAD PREDICTION OF A HIGH ASPECT RATIO COMPOSITE SWEPT WING

Andreas Hermanutz, Mirko Hornung
Institute of Aircraft Design, Technical University of Munich

Keywords: *Aircraft Aeroelasticity, Model Reduction, High AR-Wing*

Abstract

An approach for a virtual aircraft model with the purpose to simulate the static and dynamic aeroelastic behavior of a flexible aircraft is presented. To reduce the computational effort, methods for accurate model reduction and their applicability for a flexible aircraft configuration is investigated. Static and dynamic flight maneuvers are performed to identify critical load conditions, which are furhter used with the inverse transformation for detailed structural sizing. As a computational demonstration example, a generic high aspect ratio composite aircraft swept wing is used.

1 Introduction

Established wing structures have reached their capability in further improvements and wing layout, as well as the structural designs are showing only minor variations. Nowadays, modern composite designs show great potential in wing development by tailoring the wing to a specific intended behavior like passive load elevation or aeroelastic stabilization by using anisotropic stiffness properties of the structural layout. In addition, modern wing design exhibit a significant increase in wing flexibility due to extensive lightweight structural design, an increasing aspect ratio or the introduction of morphing wing technologies. The increasing wing flexibility inherently leads to more aeroelastic effects, whose influence in the structural design cannot be neglected.

Simulation technologies on structural as well as on aerodynamic side are important tools in the aircraft development process. The idea of a virtual aircraft model, which will allow virtual flight test for aircraft load prediction and performance is part of the national LuFo funded project VitAM. To investigate the aircraft behavior including elastic effects, different kinds of models are necessary.

The combination of models to a complete dynamic aeroelastic aircraft model allows the simulation and evaluation of virtual flight maneuvers e.g. take-off or gust response analysis at an early point of the development process. As described in the verification specifications CS-25, structural loading has to be proven for different flight maneuvers. Especially the evaluation of dynamic flight conditions needs a high computational effort, which is why full Finite Element (FE) models are not applicable. Reduced order modeling is investigated for the purpose of structural sizing on full aircraft level for different flight conditions. Dynamic flight maneuvers on a fast computational model are therefore used to identify critical load conditions.

1.1 Reduced Order Modelling

The motion of a structural system can be described by the discretized mass $[M]$ and stiffness matrix $[K]$ in the form

$$[M]\{\ddot{x}\} + [K]\{x\} = \{F\} \qquad (1)$$

The structural discretization is usually undertaken with the FE method and leads typically to a system of some million Degrees of Freedom (DoFs). Model order reduction is following the idea to simplify a model without losing the most important system information. The system which has to be solved is usually

reduced in its dimensions to some hundred DoFs, grouped in the so-called Analysis-Set (A-Set). The neglected DoFs are grouped in the Omitted-Set (O-Set) as exemplarily shown in the beam model in Fig. 1.

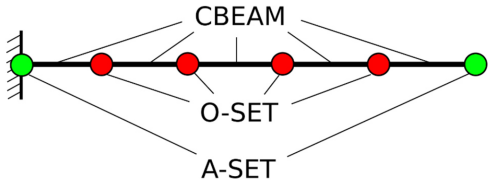

Fig. 1: DoF groups of a structural system

To transfer Equation 1 to the reduced A-Set, the linear transformation matrix $[T]$ from the full to the reduced DoF-set as shown in Equation 2 has to be computed.

$$\begin{Bmatrix}\vec{x}_a\\ \vec{x}_o\end{Bmatrix} = [T]\{\vec{x}_a\} \tag{2}$$

For the presented work different methods to construct the transformation matrix [T] for aeroelastic application are investigated:

- *Guyan-Reduction* [1]
- *Dynamic-Model-Reduction* [2]
- *Improved-Reduced-System* [3]

1.2 Guyan-Reduction Method (GRM)

The Guyan-Reduction is one of the most well-known and most commonly used reduction methods. As it considers only the stiffness matrix, and hence neglects dynamic effects, it is also referred to as a static condensation method. The static system part of Equation 1 is separated to the individual DoF-sets, so that the equilibrium equation can be rewritten as:

$$\begin{bmatrix}K_{aa} & K_{ao}\\ K_{oa} & K_{oo}\end{bmatrix}\begin{Bmatrix}\vec{x}_a\\ \vec{x}_o\end{Bmatrix} = \begin{Bmatrix}\vec{F}_a\\ \vec{F}_o\end{Bmatrix} \tag{3}$$

Solving Equation 3 with respect to the A-set leads to the transformation matrix $[T]$:

$$\begin{Bmatrix}\vec{x}_a\\ \vec{x}_o\end{Bmatrix} = \begin{bmatrix}I\\ -K_{oo}^{-1}K_{oa}\end{bmatrix}\{\vec{x}_a\} \tag{4}$$

The transformation of the mass matrix is carried out respectively. The static results are represented exactly as the GRM uses it as input. As presented in [4], errors occur due to an incorrect reduced mass representation, which in turn effects especially the dynamic characteristic.

1.3 Dynamic-Model-Reduction (DMR)

In general, the Dynamic-Model-Reduction is based on the static Guyan-Reduction, except for the mass matrix, which is included. The equation of motion is therefore transferred to modal space and can be written as:

$$\left(\begin{bmatrix}K_{aa} & K_{ao}\\ K_{oa} & K_{oo}\end{bmatrix} - \omega^2\begin{bmatrix}M_{aa} & M_{ao}\\ M_{oa} & M_{oo}\end{bmatrix}\right)\begin{Bmatrix}\vec{\phi}_a\\ \vec{\phi}_o\end{Bmatrix} = \vec{0} \tag{5}$$

As in the GRM, Equation 5 is solved to obtain the transformation matrix $[T]$ in the form:

$$\begin{Bmatrix}\vec{x}_a\\ \vec{x}_o\end{Bmatrix} = \begin{bmatrix}I\\ -(K_{oo}-\omega^2M_{oo})^{-1}(K_{oa}-\omega^2M_{oa})\end{bmatrix}\{\vec{x}_a\} \tag{6}$$

One can see from Equation 6 that the influence of the mass matrix with respect to ω is taken into account. In case of $\omega = 0\ Hz$, the DMR leads to the same result as the GMR. Major drawback is that the transformation matrix is only designed for one specific ω. For applications where several eigenmodes in a bigger range have to be included to describe the structural motion correctly, the DMR is error-prone to give a general solution.

1.4 Improved-Reduced-System (IRS)

The IRS takes the result of the static GRM model and adds an additional correction matrix to take dynamic effects into account. Details about the correction matrix are given in [3]. The transformation matrix can be expressed as follows:

$$[T_{IRS}] = [T_{GRM}] + [T_{corr}] \tag{7}$$

$$[T_{IRS}] = \begin{bmatrix}I\\ -K_{oo}^{-1}K_{oa}\end{bmatrix} + \begin{bmatrix}0\\ [K_{oo}^{-1}M_{oa} - K_{oo}^{-1}M_{oo}K_{oo}^{-1}K_{oa}][D]\end{bmatrix} \tag{8}$$

As shown in [3], the additional matrix $[D]$ can be used to neglect the frequency dependency of the DRM. The IRS transformation matrix has a significant higher computation effort, but as presented later this drawback is compensated by the higher accuracy.

2 Generic Aircraft Model

As a demonstration example, a generic transport aircraft with a high aspect ratio swept wing as shown in Fig. 2 is used. The design MTOW is 95t with the wing planform parameters as presented in Table 1.

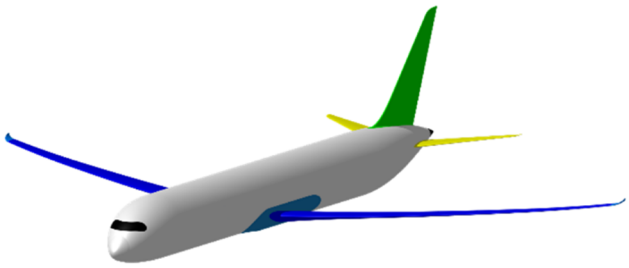

Fig. 2: Generic flexible wing aircraft configuration

Table 1: Wing planform parameters

Wing Area (S)	Aspect Ratio (AR)	Taper Ratio (TR)	Wing Sweep Λ
58 m²	14.0	0.2	25°

2.1 Structural Wing Model

The intensive use of modern composite materials is one objective for the structural design. For the main load carrying components like skin, ribs, stringer, and spars a monolithic CFRP layup is used. Leading and trailing edge devices are designed in a sandwich structure to provide the required bending stiffness against elasto-stability failure. The monolithic skin is in addition supported by 30 ribs and Ω-stringers.

For the structural model description, the FE method with a shell discretization is used. The different composite parts are modeled in overlapping areas with a smeared stiffness approach. To cover the anisotropic stiffness behavior, the classical laminate theory is used to calculate the local stiffness behavior of each element. To avoid artificial stiffness of the leading and trailing edge devices, the DoFs of the wing skin are decoupled, so that no forces or moments can be transferred via the skin into the wing box.

As the presented work considers only symmetric flight maneuvers, a half wing model is implemented. Model symmetry is enforced by symmetry boundary conditions U_{sym} as shown in Fig.3.

$$\{U_{sym}\} = [X \quad 0 \quad Z \quad 0 \quad Y_{rot} \quad 0] \qquad (9)$$

In case of static simulations, an additional elastic support at the center wing box is needed to fix all six rigid body DoFs of the aircraft. To describe a free-flying quasi-steady flight maneuver, a support spring as presented in [5] is used.

2.2 Reduction Points Definition (A-Set)

The reduced order model accuracy is, besides the model reduction method, furthermore depended on the A-Set DoFs location. For wing condensation, reduction points are defined along the span-wise direction at each wing rib. As the desired location contains not necessarily a node to attach, rigid body coupling elements are used to add an additional node. To avoid adding artificial stiffness to the model, RBE3 interpolation elements are used to define the condensation point. Fig. 4 shows the principle setup for the wing root rib.

2.3 Aerodynamic Model

The aerodynamic model is implemented with lifting elements along the structural condensation points as shown in Fig. 5. Each lifting element can be treated as a separate wing section and the aerodynamic forces are calculated with the local derivatives.

$$\mathrm{L} = q \cdot s \cdot (C_{L0} + C_{L\alpha} \cdot \alpha) \qquad (10)$$

$$M = q \cdot s \cdot c \cdot C_{M,N.P.} \qquad (11)$$

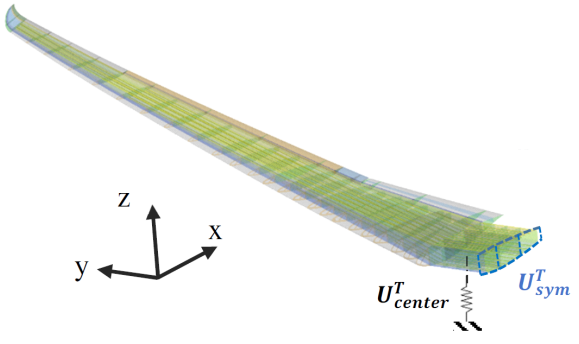

Fig. 3: Structural model and elastic wing support

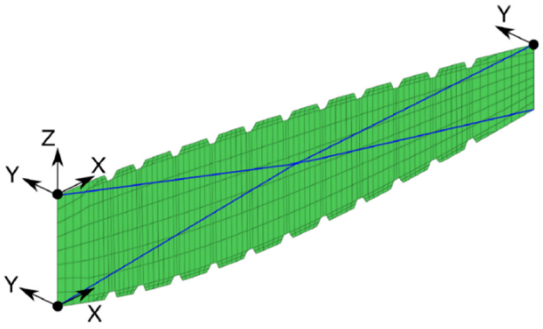

Fig. 4: Wing rib with RBE3 connection and local condensation node

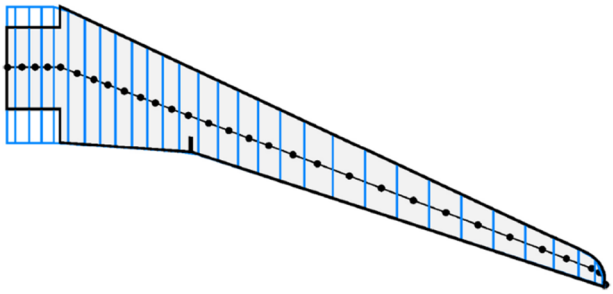

Fig. 5: Aerodynamic lifting model with span-wise distributed condensation nodes

The reduction points together with the leading and trailing edge points define the wing mid-surface. For unsteady aerodynamic modeling, the mid-surface is used as an interface. The necessary force and motion transfer over the interface can be established via a spline interpolation as e.g. presented in [6].

3 Aeroelastic Modelling

For aeroelastic modeling, it is assumed that the rigid and elastic displacement can be expressed as a sum of natural eigenvectors q

$$\{x\} = [\phi]\{q\} \tag{12}$$

With the required mass normalization of the eigenvector, the equation of motion can be transferred to modal space as shown in Equation 13, where $[I]$ represents the unity matrix.

$$[I]\{\ddot{q}\} + \begin{bmatrix} \omega_1^2 & & \\ & \ddots & \\ & & \omega_n^2 \end{bmatrix}\{q\} = [\phi]^T\{F\} \tag{13}$$

The right hand sided external force vector containing the aerodynamic forces $\{F\}$ still have to be determined. To do so, potential flow based theories such as the Doublet-Lattice Method (DLM) [7] or CFD methods as presented in [8] can be used. The projection of the aerodynamic forces on the structural eigenmodes are known as Generalized Aerodynamic Forces (GAF). As presented in [9], the frequency dependent aerodynamic loads can be approximated with a rational function approximation so that the aerodynamic model can be expressed in the form

$$\{F_{Aero}\} = [\hat{A}_0]\{q\} + \frac{c}{V}[\hat{A}_1]\{\dot{q}\} + \sum_{n=2}^{k}[\hat{A}_n]\{q_{l_n}\} \tag{14}$$

which is dependent on motion $\{q\}$, the velocity $\{\dot{q}\}$ and a given number of lag states $\{q_{l_n}\}$.

3.1 Time Integration and Solver Description

After the system equation of the aeroelastic model is assembled, an appropriate numerical solver for the decoupled partial differential equation is used. As the system matrix is stiff, an implicit time integration scheme with the advantage of greater time steps is used. Due to its low computational effort and preferred choice in structural dynamics, a modified New-Mark-Beta method is used.

$$[A_1]\{\vec{U}_{t+\Delta t}\} = \vec{A}_2 + [A_3]\{\vec{U}_t\} + [A_4]\{\vec{U}_{t-\Delta t}\} \tag{15}$$

$$[A_1] = \left[\frac{M}{\Delta t^2} + \frac{D}{2\Delta t} + \frac{K}{3}\right] \tag{16}$$

$$\vec{A}_2 = \frac{1}{3}[\vec{F}_{t+\Delta t} + \vec{F}_t + \vec{F}_{t-\Delta t}] \tag{17}$$

$$[A_3] = \left[\frac{2M}{\Delta t^2} - \frac{K}{3}\right] \tag{18}$$

$$[A_4] = \left[-\frac{M}{\Delta t^2} + \frac{D}{2\Delta t} + \frac{K}{3}\right] \tag{19}$$

The main differences to the standard New-Mark-Beta-Method is a formulation, where the dynamic forces are averaged over the last three time steps and a modification of the stiffness matrix $[K]$ in a way that for a system with no mass and damping the numerical solution represents the static problem formulation.

After solving for the displacement field, the velocity and acceleration vectors are obtained via the finite difference schemes.

$$\{\vec{U}_t\} = \frac{1}{2\Delta t}(\vec{U}_{t+\Delta t} - \vec{U}_{t-\Delta t}) \quad (20)$$

$$\{\ddot{\vec{U}}_t\} = \frac{1}{\Delta t^2}(\vec{U}_{t+\Delta t} - 2\cdot\vec{U}_t + \vec{U}_{t-\Delta t}) \quad (21)$$

3.2 Static Reduced Order Model Comparison

To compare the different reduction methods and their accuracy, the static result of the full FE model to the reduced order model is used. As reference load case, steady flight with $Ma = 0.3$ at an altitude of 1.0 km is used. As observation point, the maximum static tip deflection is selected.

Table 2: Static displacement values and their deviations

Displacement		Deviation		
DOF	Full FEM	GRM	DRM	IRS
u_x	458,6	0.0 %	0.0 %	0.0 %
u_y	-1272,4	-0.00031%	-0.00031%	-0.00031%
u_z	9246,6	-0.00025%	-0.00030%	-0.00025%
rot_x	0,664	-0.00039%	-0.00048%	-0.00039%
rot_y	-0,217	-0.00060%	-0.00078%	-0.00060%
rot_z	-0,054	-0.00043%	-0.00052%	-0.00043%

As one can see from Table 2, no significant deviations in case of the static reduction compared to the full FE model can be observed. This result was expected, as all three methods aim to represent the static case exactly. The occurrence of small errors can be explained by numerical round-offs, data transfer errors within the different sub-tools in the simulation chain and the RBE3 interpolation elements.

Observing the total deflection of the wing, one can realize that the total deflection with over $u_{max} > 9[m]$ is quite high with respect to the overall wing dimensions. Because there is no aerodynamic coupling present in this comparison study, the wing wash-out, and therefore its inherent load reduction capability, is not considered.

The result for a full coupled aeroelastic system is shown in Fig. 6. One can see that the aerodynamic interference with the structure changes the structural response significantly. With increasing elasticity effects, these effects get more deciding. For this reason, they cannot be neglected in an early design stage.

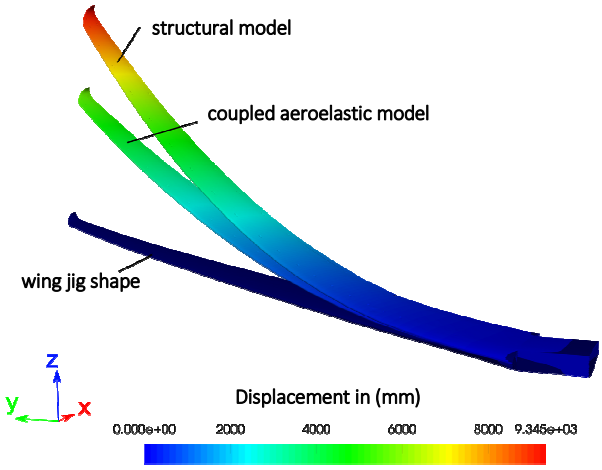

Fig. 6: Displacement result for the structural and aeroelastic model

3.3 Dynamic Reduced Order Model Comparison

The modal properties are used to compare the dynamic behavior of the full and the reduced model. As in the static case, the natural frequencies and eigenvectors are compared to the full model.

The deviations of the first ten elastic natural frequencies are shown in Table 3. All reduction methods show a good approximation capability for the lower eigenmodes. GRM and DRM are losing accuracy at higher modes. Only the IRS method keeps the error in an acceptable range.

Table 3: Deviation of the first twelve natural elastic frequencies

EM	GRM	DRM	IRS
1	0.0059%	0.0003%	0.0017%
2	0.1035%	0.0852%	0.0002%
3	0.0116%	0.0106%	0.0005%
4	0.4334%	0.4168%	0.0001%
5	2.3620%	2.3324%	0.0022%
6	1.4476%	1.4300%	0.0011%
7	1.7861%	1.7801%	0.0185%
8	3.6551%	3.6379%	0.0319%
9	8.5736%	8.5500%	0.1309%
10	13.7807%	13.7614%	0.5728%

As the aerodynamic reaction is strongly dependent on the wings elastic deformation and due to the modal transformation, the resulting eigenmodes are evaluated between full and reduced model. To get a quantitative value, the Modal Assurance Criterion (MAC) as defined in Equation 22 is used to compare the parallelism of the eigenvectors ϕ_i.

$$MAC = \frac{|\phi_{full} \cdot \phi_{red}|^2}{|\phi_{full}| \cdot |\phi_{red}|} \tag{22}$$

The result of each method is shown in Figures 6-8. As for the natural frequencies, the eigenmodes match well in the lower frequency range, indicated by values close to 1.0 on the main diagonal. The computational effort is higher for determining the transformation matrix for the IRS method, but as higher accuracy can be reached, the IRS method is the preferred choice and therefore used for further aeroelastic simulations.

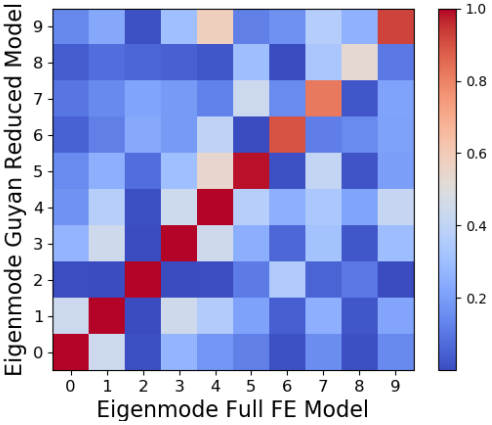

Fig. 7: MAC criteria for the GR method

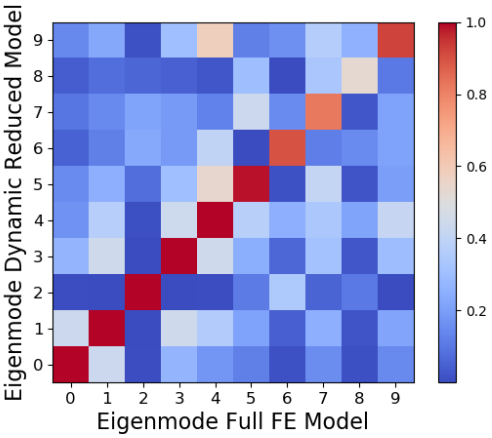

Fig. 8: MAC criteria for the DR method

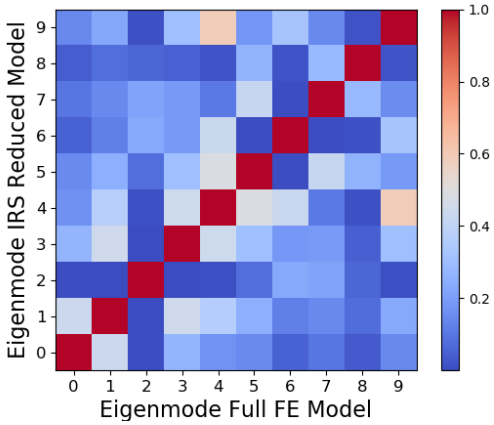

Fig. 9: MAC criteria for the IRS method

4 Aeroelastic Simulations

After the aeroelastic model setup is completed, the simulation purpose of virtual flight maneuvers can be executed. As no flight controller is in the presented virtual model implemented, rigid body motion is considered through a pre-defined flight path.

The final objective is to determine critical load conditions by observing the maximum displacement or acceleration values. As the transformation matrix is known, the internal loads of the structure can be transferred back to the full FE model and a detailed stress analysis for the critical condition can be performed. With the 6x6 constitutive matrix, the internal stress is related to the strains in matrix notation as follows:

$$\{\sigma\} = [C]\{\varepsilon\} \tag{23}$$

The strains which are depending on the displacement field are transferred back to the full model. In matrix notation with the linear differential operator matrix $[L]$ follows:

$$\{\varepsilon\} = [L]\{x_{full}\} \tag{24}$$

$$\{\varepsilon\} = [L][T]\{x_{red}\} \tag{25}$$

The structural responses on two typical flight maneuvers, computed on the reduced ILS model are presented in the following two chapters.

4.1 Virtual Take-Off Maneuver

The simulation of a virtual take-off maneuver with flexible wings is divided into three simulation steps: acceleration, rotation, and climb as shown in **Fig. 10**.

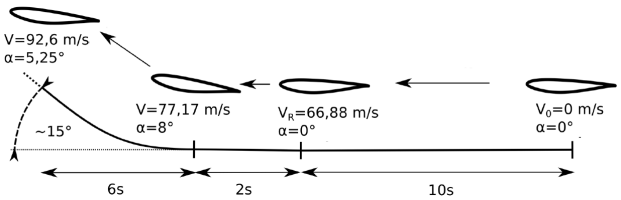

Fig. 10: Take-Off maneuver

The time discretization is chosen to resolve the most important eigenmodes with:

$$\Delta t = \frac{1}{20 \cdot f_{max}} \tag{23}$$

The maximum frequency of interest is $f_{max} = 30Hz$. The time step size is therefore set to $\Delta t = 0.001s$.

The wing tip's structural response due to the maneuver loading is shown in Fig. 11. After the aircraft has accelerated and the rotation has ended, the displacement response descends into a quasi-steady climb with a short transient overshoot.

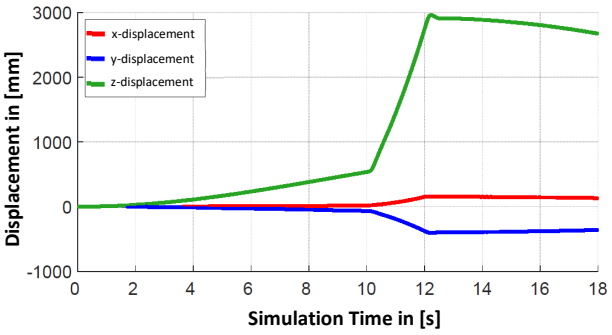

Fig. 11: Wing displacement response

4.2 Virtual 1-cos Gust Response

Besides the aircraft maneuver loads, turbulences and discrete gusts are additional loads that the aircraft has to withstand. The mathematical 1-cos gust velocity defined in Equation 24 is (according to the CS-25) a required load case, which has to be proven in the certification process.

$$v_g(t) = \frac{v_{g0}}{2}\left(1 - \cos\left(\frac{2\pi V}{l_g}t\right)\right) \tag{24}$$

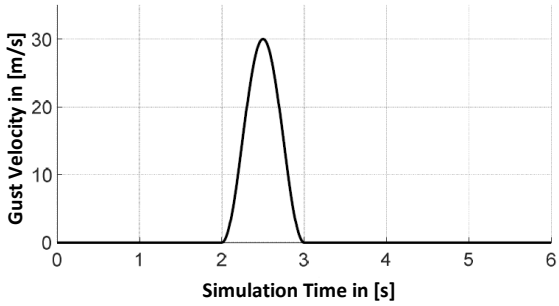

Fig. 12: 1-COS gust velocity

In Fig. 13 and 14, the structural displacement and acceleration response of the wing for different gust-gradients is presented. All responses show a harmonic characteristic. For higher gust-gradients, the wing reacts with higher bending as for lower gust-gradients due to the additional lift caused by the increased local AoA of the gust. With the wing sweep and the inherent bending-torsion coupling, the wing has an increased natural passive load alleviation characteristic, compared to less slender wings. The lower skin stress for the maximum load condition is as example shown in Fig.15. As can be observed, the experienced internal loading is reduced.

The opposite behavior can be observed for lower gust-gradients. Inertia effects start dominating and the wing has no time to deflect. As the out-of-plane wing bending is smaller, the aerodynamic damping is also reduced, which is why the wing starts to vibrate for a longer time range. The smaller the gust-gradient becomes, the closer the reaction can be described as an impulse excitation on the structure. As the gust energy is not transformed into internal structural energy, the aircraft experiences higher acceleration, what effects directly the flight dynamics.

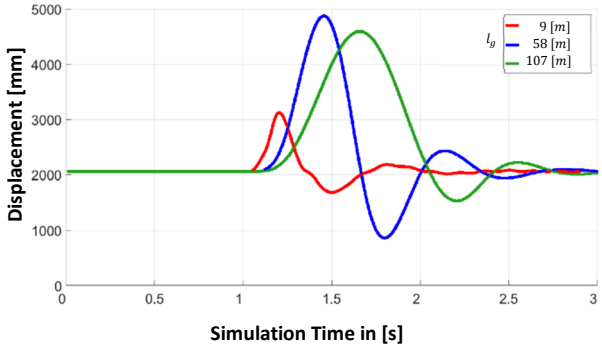

Fig. 13: 1-COS wing displacement response depending on the gust-gradient

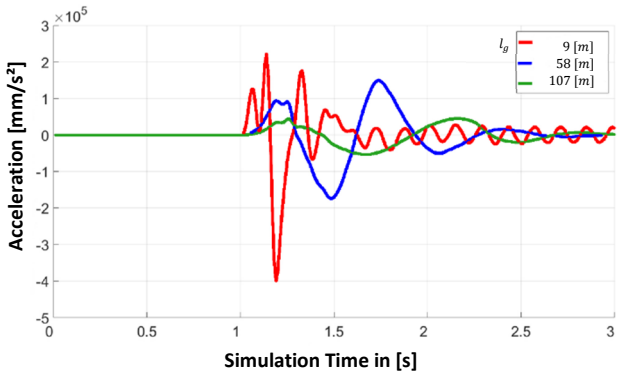

Fig. 14: 1-COS wing acceleration response depending on the gust-gradient

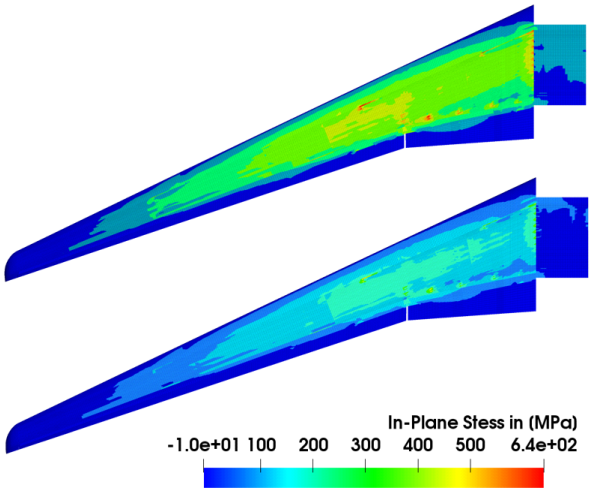

Fig. 155: Lower skin stress level comparison for medium gust gradient (upper) and higher gust gradient (lower)

5 Conclusion and Future Work

Different reduction methods are presented and proven for their ability to approximate a flexible aircraft structure. The IRS method shows the highest amount of computational effort but delivers the most accurate results for dynamic simulations.

A high aspect ratio transport aircraft wing was used to present the computational methods. Elastic effects, especially wing torsional-bending coupling, and the need to consider them in an early design stage is demonstrated.

The applied aeroelastic model represents a minimum on necessary model requirements, which are needed to investigate the aircraft behavior. In future work, the model will be extended with additional flap modes, which enables it to include a flight controller. The aircraft's rigid motion is then no longer enforced by the flight path, which leads to a deeper insight and therefore to an increased knowledge level of the configuration. Furthermore, flight controllers are usually developed on a rigid a/c configuration. As the reduced model is fast enough, the aeroservoelastic behavior can be further studied with a flexible configuration.

References

[1] R. J. Guyan, „*Reduction of stiffness and mass matrices,*“ AIAA Journal, Bd. 3, Nr. 2, p. 380, 1965.

[2] P. Salvini und F. Vivio, “*Dynamic reduction strategies to extend modal analysis approach at higher frequencies”*, University of Rome, 2007.

[3] J. H. Gordis, “*An analysis of the Improved Reduced System (IRS) model reduction procedure”*, U.S. Naval Postgraduate School, 1994

[4] M. I. Friswell and J. E. Mottershead, „*Finite Element Model Updating in Structural Dynamics*“, Springer, 1995, p. 68

[5] A.Hermanutz and M.Hornung, “*High Fidelity Trim Calculation Under Consideration of Aeroelastic Effects of a High Aspect Ratio Swept Wing*”, IFASD-2017, Como Italy

[6] MSC.Nastran, “Aeroelastic Analysis User Guide”, MSC Software Corporation

[7] Albano, E. and Rodden, W., “*A Doublet-Lattice Method for Calculating Lift Distributions on Oscillating Surfaces in Subsonic Flows*”, AIAA Journal, Vol. 7, No. 2, 1969, pp. 279–285

[8] V.Rozov and A.Hermanutz, “Aeroelastic Analysis of a Flutter Demonstrator With a Very Flexible High Aspect Ratio Swept Wing”, IFASD-2017, Como Italy

[9] Sherwood H. and William M., *“Nonlinear Programming Extensions to Rational Function Approximation Methods for Unsteady Aerodynamic Forces”*, NASA Technical Paper 2776, July 1988

Copyright Statement

Contact Author Email Address

Andreas Hermanutz, Research Associate
Technical University of Munich,
Institute of Aircraft Design
andreas.hermanutz@tum.de